Electronic and optical properties of aluminium-doped anatase and rutile TiO_2 from *ab initio* calculations

Raphael Shirley and Markus Kraft*
Department of Chemical Engineering and Biotechnology, University of Cambridge, New Museums Site, Pembroke Street, Cambridge CB2 3RA, United Kingdom

Oliver R. Inderwildi
Smith School for Enterprise and the Environment, University of Oxford, Hayes House, 75 George Street, Oxford OX1 2BQ, United Kingdom

(Received 29 April 2009; revised manuscript received 19 January 2010; published 17 February 2010)

The electronic-structure and optical properties of aluminium-doped rutile and anatase TiO_2 have been investigated using density-functional theory with plane-wave basis sets and pseudopotentials. This was done using the periodic supercell method as implemented within the CASTEP software package with Al concentrations approaching the very low levels present in industrial samples of rutile TiO_2. Defect states involving substitution of a titanium atom for an aluminium atom were studied along with the more stable configuration of two adjacent aluminium substitutions with an oxygen vacancy in between. In the latter case, aluminium does not introduce band-gap states but leads to an increase in the band gap in both anatase and rutile. This suggests that aluminium doping pushes the absorption edge further into the UV and therefore reduces the photocatalytic activity. Single oxygen vacancies in anatase were also studied. Reactions to form the most stable defects are exothermic for both phases. Finally, migration of aluminium in both phases is investigated. Migration transition states are found to have a significantly lower energy in rutile. At industrially relevant temperatures, overcoming the barrier to migration is probably only possible in rutile.

DOI: 10.1103/PhysRevB.81.075111 PACS number(s): 71.20.Nr, 78.20.Ci

I. INTRODUCTION

Titanium dioxide (TiO_2) is widely used as a pigment, as a catalyst support, and as a photocatalyst. The combustion of titanium tetrachloride ($TiCl_4$) to synthesize TiO_2 nanoparticles is a multimillion ton per year industrial process.[1] In this "chloride" process, purified titanium tetrachloride is oxidized at high temperatures (1500–2000 K) in a pure oxygen plasma or flame to produce TiO_2 particles.[2–5] In many industrial reactors, a small amount (less than 1% by mass) of vaporized $AlCl_3$ is also added. This is done to promote the formation of the rutile phase of TiO_2 and to increase the photostability of the resulting particles. Al is believed to act as a low-concentration dopant within the TiO_2 crystal but the reason it influences crystal mode is not known. It seems as many authors have suggested it hinders the anatase-rutile transformation[6,7] as say the opposite.[8,9] Shirley *et al.* investigate the early stage gas phase chemistry to see if phase might be determined by the nucleation process but there seems to be very little chemical interaction.[10]

TiO_2 crystallizes in three different forms: rutile, anatase, and brookite. Rutile and anatase are the two most stable forms and are both produced on an industrial scale. They are both investigated here. Both systems are tetragonal and fully described by three parameters: a, c, and u. The parameters a and c are shown in Fig. 1, u defines the fractional coordinate of the O atom. The formal space groups are given in Table II.

Steveson *et al.*[11] presented a theoretical study into the defect states of Al-doped TiO_2. A later theoretical study by Islam *et al.*[12] went on to investigate some of the physical properties of the doped rutile phase. However, this work did not present the optical properties of this doped rutile and did not consider the anatase phase at all. While Al is added in order to promote the rutile phase, it only completely stops anatase formation at relatively high concentrations. Manufacturing aluminium-doped anatase is therefore a possibility but an understanding of the effect of Al on this phase is still lacking. There do exist a number of experimental measurements of the electronic and optical properties of TiO_2. These include total electron yield spectroscopy,[13] electron energy-loss spectroscopy,[14–17] x-ray absorption spectroscopy,[18–20] x-ray emission spectroscopy,[21] x-ray photoelectron spectroscopy,[14,22,23] wavelength-modulated transmission spectroscopy,[24] ultraviolet photoelectron spectroscopy,[25] photoluminescence spectroscopy,[26] and resonant ultraviolet photoelectron spectroscopy. With recent increases in computational power, *ab initio* methods such as density-functional theory (DFT) (Ref. 27) and Hartree-Fock (HF) have become available. These calculations have been performed with DFT and the local-density approximation (LDA),[15,22,28–33] and using the HF approach.[34] There have also been some self-consistent calculations done with the linear muffin-tin orbital

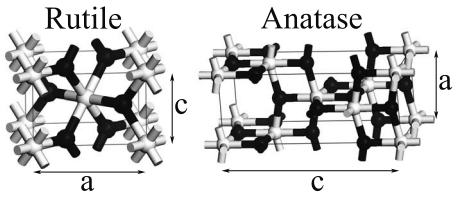

FIG. 1. Unit cells of rutile and anatase phase TiO_2. Titanium atoms are white and oxygen atoms are black. Note that this anatase cell is not the primitive cell. This unit cell is shown because it is the standard representation.

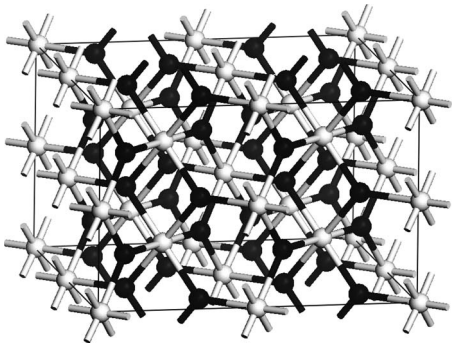

FIG. 2. Standard-size rutile supercell ($Ti_{16}O_{32}$). Titanium atoms are white and oxygen atoms are black.

method,[13,21,35–37] with tight-binding models[38–40] and with the extended Huckel molecular-orbital method.[17] A full overview of work done in the field is given in Ref. 27.

The first aim of this paper is to investigate the influence that Al doping has on the energetics, electronic structure, and optical properties of both the rutile and anatase phases of TiO_2. The second aim is to understand the processes by which Al atoms move around the lattice in both phases. This is vital for a proper understanding of the material itself and also of the processes used for its production on a large scale.

II. COMPUTATIONAL METHOD

The CASTEP (Ref. 41) density-functional software package is used throughout, this is widely used for a variety of crystal systems and has been successfully applied to TiO_2.[42,43] Specifically, it has been used for investigating the impact of dopants on electronic structure.[44,45] The generalized gradient approximation (GGA) as proposed by Perdew, Burke, and Ernzerhof (PBE) was applied,[46] combined with Vanderbilt ultrasoft pseudopotentials.[47] The plane-wave basis set was truncated at a kinetic energy of 380 eV. This value was chosen after a full convergence study from 100 to 700 eV. The electronic energy of the rutile unit cell falls by less than 1 kJ/mol between a cutoff of 380 and 700 eV. Equally, enthalpies of formation calculated by various reaction schemes do not differ by more than 1 kJ/mol over the same interval. Most importantly, the band gap is not greatly sensitive to cutoff; for pure rutile the band gap calculated using a 380 eV cutoff is 0.002 eV lower than that calculated using 700 eV. The errors due to basis-set truncation are therefore small compared to inherent errors associated with DFT. Computational time goes up linearly with the cutoff. For the smallest anatase supercells, a $7\times7\times3$ Monkhorst-Pack grid[48] is used for Brillouin-zone sampling, which is also within convergence. For the larger supercells, a $3\times3\times3$ grid is used, again well within convergence. All calculations are spin polarized in order to describe magnetic effects correctly. In order to minimize the errors due to interaction of defects moderately large periodic supercells were used up to $Ti_{16}O_{32}$ (see Fig. 2).

One $Ti_{32}O_{64}$ supercell was investigated but it took over 64 cpu days to relax the geometry and only reduced the interaction between defects by 10 kJ/mol. Even with these relatively high Al concentrations compared to the industrially produced material there seems to be little interaction between adjacent defect states; the energy of a single defect differed by 24 kJ/mol between a Ti_8O_{16}-sized and a $Ti_{16}O_{32}$-sized supercell. In order to calculate the energies of atomic Ti, Cl, O, and Al and of the molecules $TiCl_4$, $AlCl_3$, O_2, and Cl_2, the species are placed in the center of a $15\times5\times15$ Å cell in order to ensure negligible interaction between neighboring molecules. Supercells were used for molecular energies in order to use the same method (with the same cutoff energies, etc.) throughout and to maximize cancellation of errors.

Enthalpies of formation are calculated for one unit cell using Eq. (1) and any comparisons are made between equivalent size supercells. The error with respect to experiment in Table I is partly due to the zero-point vibrational energy, which was only calculated here for pure anatase and rutile and is shown in brackets in Tables I and II. The enthalpy of reaction calculated from Eq. (2) provides an equivalent comparison of stability as the defect formation energy, which we will use later as a useful measure of the stability of a defect,

$$x\mathrm{TiCl_4} + \frac{y}{2}\mathrm{O_2} + z\mathrm{AlCl_3} \rightleftharpoons \mathrm{Ti}_x\mathrm{O}_y\mathrm{Al}_z(s) + \left(2x + \frac{3}{2}z\right)\mathrm{Cl_2}, \tag{1}$$

TABLE I. Comparison between computational methods and experiment for bulk properties of rutile (point group D_{4h}^{14}, space group $P4/mnm$). The brackets after the enthalpy show the zero-point vibrational energy as calculated using norm-conserving pseudopotentials.

	GGAPBE	PWGGA (Ref. 12)	PW1PW (Ref. 12)	MSINDO (Ref. 11)	Expt.
a (Å)	4.67	4.63	4.59	4.49	4.594[a]
c	2.97	2.98	2.98	2.88	2.958[a]
u	0.305	0.305	0.305	0.299	0.305[a]
E_a (kJ/mol)	−1932 (+20)	−2054	−1929	−1875	−1915[a]
E_g (eV)	1.86	1.90	3.54		3.03[b]

[a]Reference 49.
[b]Reference 26.

TABLE II. Comparison between computational methods and experiment for bulk properties of anatase (point group D_{4h}^{19}, space group $I4/amd$). The brackets after the enthalpy show the zero-point vibrational energy as calculated using norm-conserving pseudopotentials.

	GGAPBE	HF (Ref. 50)	LDA (Ref. 51)	MSINDO (Ref. 11)	Expt.
a	3.80	3.763		3.697	3.785[a]
c	9.67	9.851		9.006	9.514[a]
u	0.207	0.202		0.2057	0.2066[a]
E_a (kJ/mol)	−1940 (+22)			−1904	−1895[b]
E_g (eV)	2.25		2.04		3.20[c]

[a]Reference 52.
[b]Reference 53.
[c]Reference 54.

$$(x+z)\mathrm{TiO_2}(s) + z\mathrm{AlCl_3} + \frac{z}{2}\mathrm{Cl_2} \leftrightharpoons \mathrm{Ti}_x\mathrm{O}_y\mathrm{Al}_z(s) + z\mathrm{TiCl_4} + \left(x+z-\frac{y}{2}\right)\mathrm{O_2}. \quad (2)$$

There is good agreement between the method used here and experiment and indeed with the other theoretical calculations performed on anatase[50,51] and rutile.[11,12,26,49] This strong agreement for bulk properties is encouraging. The significant underestimation of the band gap is a concern. However, it does seem to be well behaved, consistently underestimating the gap by 50%.

The transition state searches reported in Sec. IV D were carried out using a full linear synchronous transit/qudratic synchronous transit search with intermediate conjugate gradient refinements. This method is described in detail by Govind *et al.*[55] Refinement is considered complete when the forces on every atom are under 0.05 eV/Å.

III. DEFECT STRUCTURES

The defect structures investigated here are the most stable defect states as found by Steveson *et al.*[11] using semiempirical quantum calculations on large clusters of TiO_2. All these structures are shown in Fig. 3. While the errors associated with Steveson's calculations are large (up to 50 kJ/mol), the most stable crystal structures were over 500 kJ/mol more energetically favorable. These states consist of either direct substitution of a titanium atom for an aluminium atom (anatase model 1 and rutile model 1) or double substitution of two titanium atoms with an oxygen vacancy in between (anatase models 2–3 and rutile model 2). Interstitial defects were found to be comparatively unstable in agreement with Ref. 11 and so physical properties were not calculated for them. This is in agreement with Ref. 56 where experimental nuclear-magnetic-resonance studies suggest the prevalence of Ti substitution in Al-doped rutile. It is not entirely clear how mobile an Al defect is. The diffusivity of Al through the TiO_2 lattice is unknown. A study into this process would be helpful in determining the likelihood of two Al defects coming together with an O vacancy at the temperatures involved in commercial synthesis. If this process is slow and these interstitial states are present in the lattice then the nucleation seed must be responsible for the crystal structure.

IV. RESULTS

A. Band structures

While DFT is known to underestimate band gaps by up to 50% (Ref. 57), it is possible to make qualitative statements regarding the influence of dopants.[58] See Table II in Ref. 12 in which the band structures from a pure DFT calculation agree with the hybrid calculations and differ only by a constant value across k space. The LDA+U method[59] is known to be able to correct band-gap errors by applying a potential to the outer d electrons of transition metals. It is possible to theoretically calculate the on-site coulomb potential U (Ref. 60) but it is more common to vary it empirically depending on the property of interest.

This method was investigated but the relationship between band gap and the Hubbard U potential was found to be dependent on the crystal phase (see Fig. 4). Since we do not have accurate experimental measurements of the band gaps of the Al-doped system and because we are interested in the

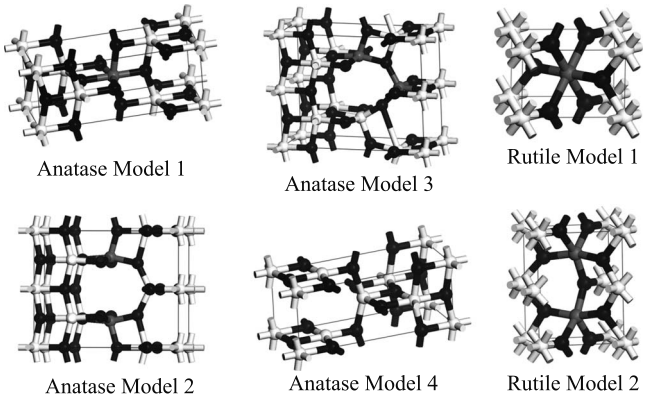

FIG. 3. Defect states of rutile and anatase phase TiO_2 that are considered in this paper. Titanium atoms are white, oxygen atoms are black, and aluminium atoms are gray. Minimum-size supercells are shown to aide clarity. The rutile models are included primarily for validation of the method since they have already been studied by Islam *et al.* (Ref. 12).

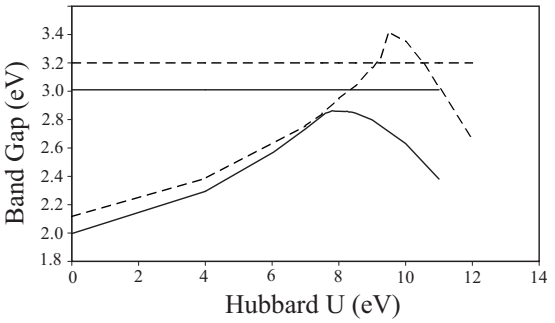

FIG. 4. Relationship between band gap of rutile (solid line) and anatase (dashed line) phases and the Hubbard U parameter. Horizontal lines indicate the experimental values for rutile (Ref. 26) and anatase (Ref. 54).

qualitative impact of dopants on the band gap it was decided that the LDA+U method was not useful here. The effect of U on the band gap of both phases is included here in order that other researchers who are studying the undoped system might benefit from these calculations. Additionally, the band gap is closest to the experimental value at around 7 eV. This is worryingly large and implies that there may be some physical process that cannot be explained by adding a fixed potential to the titanium d electrons. A similar value of 8.1 eV was found by Perebeinos *et al.*[61] in their study of TiF_3. Clearly, this method is not well suited to the Ti 3d orbital.

Band structures are calculated along the path with the most high-symmetry points, which are labeled as in Ref. 62. The PBE functional predicts rutile to have a direct gap at Γ in agreement with Islam.[12] Interestingly the same computational method implies that anatase has an indirect gap with the top of the valence band at M and the bottom of the conduction band at Γ. This is in agreement with the linear muffin-tin orbital calculations of Mo and Ching[51] and with GGA calculations on pure anatase by Qiang.[63] Table III shows the minimum direct and indirect band gaps for the standard-size supercells of anatase models 1–4. In the case of anatase model 4, the solitary oxygen vacancy causes the Fermi energy to move into the conduction band, which explains the observed coloring of oxygen-deficient anatase.[27]

B. Optical properties

CASTEP calculates optical properties from the dielectric function, the imaginary part of which can be calculated directly from the full many-electron wave function. The real part is then determined via a Kramers-Kronig transform. The imaginary and real parts of the refractive index are calculated in the polarization direction (1 0 0). Other directions were investigated and it was found that trends, with respect to defect states, in the value of the refractive index were maintained in different polarizations. The dielectric functions of both rutile and anatase are highly anisotropic in the pure and defect states. The real part of the refractive index of rutile ranged from having a maximum of 3.5 in the polarization (1 0 0) to having a maximum of 4.5 in the polarization (1 1 1). The optical properties are determined by the band gap and so its underestimation by DFT will lead to significant errors. The refractive index will be overestimated. These can be removed by correcting the gaps empirically. However, here we are interested in trends due to the defects so we will not correct band gaps. For this reason our calculations will all predict an absorption edge at unrealistically high wavelengths. In both anatase and rutile, the defects lead to a lowering in the refractive index across the visible range. The unpaired electron introduced by direct substitution of Ti for Al will turn the material into an n-doped semiconductor and this electrical conductance leads to a nonzero imaginary refractive index (absorption) at higher wavelengths.

C. Aluminium-doped anatase

The calculations performed on rutile show that the method here is in agreement with Islam *et al.*[12] Identical calculations were repeated on all the anatase models presented in Fig. 3. Table IV gives an overview of the relative stability of the various defect states. Most significantly it shows no significant thermodynamic bias between the phases. We will now discuss each model in turn. The CASTEP output files for all of the models discussed are available from the electronic physics auxiliary publication service (supplementary material).[64]

1. Anatase model 1

A single substitution site will lead to a valence-band hole and will have an effect on the conductivity and color. These defects are not as stable as models 2 and 3 according to the PBE calculations presented here (see Table IV). The defect formation energy is 26 kJ/mol. The reaction in which two Al substitutions (as in anatase model 1) would come together and release one oxygen atom as molecular O_2 forming one anatase model 2 is exothermic and would release 76 kJ/mol. This is in contrast with rutile where the single substitution

TABLE III. Energy gaps of direct and indirect transitions in the defective anatase states from GGA-PBE.

Model	E_g/eV (direct)	k point	E_g/eV (indirect)	k points (VB→CB)
Pure anatase (Ti_4O_8)	2.25	Γ	2.11	M→Γ
Anatase model 1($Ti_{15}Al_1O_{32}$)	1.99	Γ	1.99	Γ→Γ
Anatase model 2 ($Ti_{14}Al_2O_{31}$)	2.30	Γ	2.30	Γ→Γ
Anatase model 3 ($Ti_{14}Al_2O_{31}$)	2.33	Γ	2.33	Γ→Γ
Anatase model 4 ($Ti_{16}O_{31}$)	2.26	Γ	2.26	Γ→Γ

TABLE IV. The total electronic energy, E_{tot}, enthalpy of formation using reaction 1, $\Delta H^{0\ K}_{reac\ 1}$, and enthalpy of defect formation using reaction 2, $\Delta H^{0\ K}_{reac\ 2}$. Also included are the interstitial models shown in Figs. 7 and 8. Values for the pure states that were calculated using smaller supercells are shown above a numerator in order to aid comparison. Precise energies and geometries for all these models are included as supplementary material (Ref. 64).

Model	E_{tot} (eV)	$\Delta H^{0\ K}_{reac\ 1}$ (kJ/mol)	$\Delta H^{0\ K}_{reac\ 2}$ (kJ/mol)
Pure rutile (Ti_2O_4)	−39703/8	−2296/8	0
Rutile model 1 ($Ti_{15}Al_1O_{32}$)	−38154	−2306	−9
Rutile model 2 ($Ti_{14}Al_2O_{31}$)	−36171	−2325	−28
Rutile model I1 ($Ti_{16}Al_1O_{32}$)	−39762	−1913	527
Pure anatase (Ti_4O_8)	−39705/4	−2425/4	0
Anatase model 1 ($Ti_{15}Al_1O_{32}$)	−38155	−2399	26
Anatase model 2 ($Ti_{14}Al_2O_{31}$)	−36172	−2456	−31
Anatase model 3 ($Ti_{14}Al_2O_{31}$)	−36172	−2450	−25
Anatase model 4 ($Ti_{16}O_{31}$)	−39265	−1934	492
Anatase model I1 ($Ti_{16}Al_1O_{32}$)	−39762	−1944	633
Anatase model I2 ($Ti_{16}Al_1O_{32}$)	−39761	−1901	676

state is thermodynamically favored to the pure phase. Anatase model 1 is therefore the only system investigated here that is less stable than the pure phase. In the systems with an unpaired electron, the up-spin and down-spin bands no longer overlap due to the differing interaction between the two spin states and the outermost band. This defect leads to relatively small changes in the atomic positions compared to the states involving an oxygen vacancy. This means the relaxation energies are not very large. This is expected simply because the bonding structure does not change. Figure 5(c) shows the band structure of anatase model 1; the Fermi energy lies within the band and hence the material is conductive according to our calculations.

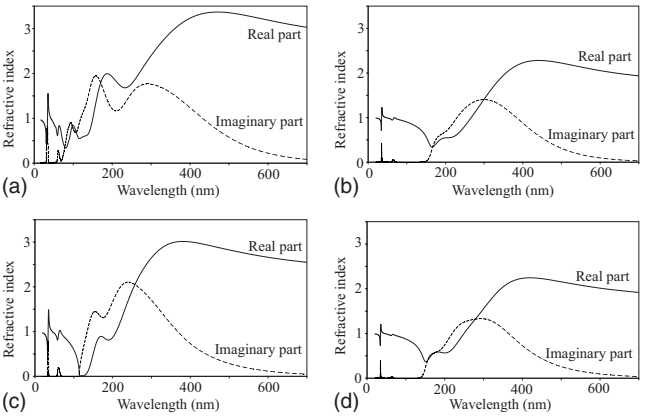

FIG. 6. Refractive indices of doped and undoped rutile and anatase using a $Ti_{16}O_{32}$ supercell. The polarization is (1 0 0). The solid line shows the real part and the dotted line shows the imaginary part. (a) Pure rutile, (b) rutile model 2, (c) pure anatase, (d) anatase model 2.

2. Anatase model 2

Substitution of one Ti^{4+} by Al^{3+} leads to a formal charge of −1 per unit cell but in anatase models 2 and 3, two Al substitutions combine with the oxygen vacancy to maintain overall charge. Models 2 and 3 represent the most stable defect structures by 50 kJ/mol per $Ti_{16}O_{32}$ supercell. It is significantly more stable than lone oxygen vacancies; by 520 kJ/mol per $Ti_{16}O_{32}$ supercell. This extreme thermodynamic prejudice would cause the Al defects to "mop up" the oxygen vacancies and reduce coloring exactly as is predicted for rutile by Islam *et al.*[12] It is interesting to observe that many trends are identical across both phases of TiO_2. The refrac-

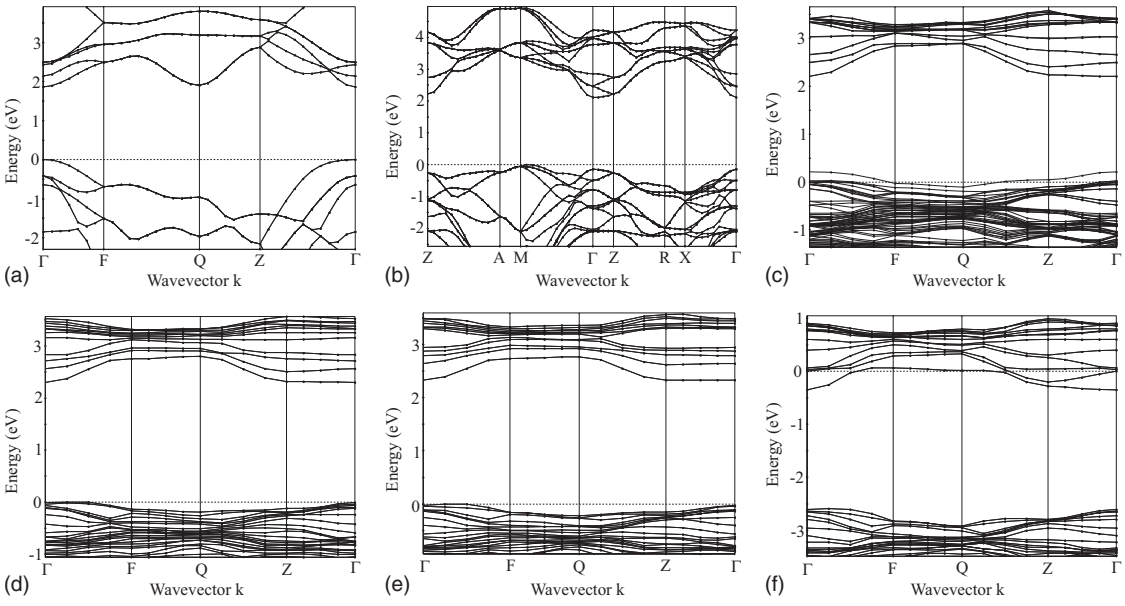

FIG. 5. Band structures calculated with one dopant site in a $Ti_{16}O_{32}$ supercell. The dashed horizontal line shows the Fermi energy, which is set as zero. (a) Pure rutile, (b) pure anatase, (c) anatase model 1, (d) anatase model 2, (e) anatase model 3, (f) anatase model 4.

tive index for model 2 is given in Fig. 6(d). The refractive index is lower across all wavelengths for each of the aluminium-doped states.

3. Anatase model 3

The impact of this defect state is very similar to that of anatase model 2 owing to the structural/electronic similarity. The band gap is increased due to the increase in the bottom of the conduction band. The relaxation energy associated with this defect is 380 kJ/mol. The second closest oxygen atoms move 1.6 Å from their positions in the pure phase. The titanium atom closest to both of the aluminium atoms moves closer to the closest aluminium atom by 0.1 Å. This stabilization shows that aluminium doping in anatase is not thermodynamically prohibited. This implies that Al is more likely to influence phase during the nucleation process.

4. Anatase model 4

It is well known that TiO_2 is usually slightly reduced[27] and so lone oxygen defects were also considered in anatase. This leads to an unpaired electron in the primitive cell and in the absence of additional defects will turn the material into a conductor and color the material. An effect observed in many experimental studies.[65] Our calculations suggest this state will overlap with the top of the valence band as opposed to the situation in rutile in which isolated states are introduced into the band gap. It is not clear why this is the case. Some relaxation takes places in the case of lone oxygen vacancies (38 kJ/mol). The adjacent oxygen atoms move toward the vacancy with the adjacent titanium atoms moving away. This suggests that the vacancy is relatively positive as might be expected given the removal of the oxygen with formal negative charge. It is well known that these oxygen vacancies form recombination centers that reduce photocatalytic activity. The lack of electronic charge may be responsible for the defects interaction with excitons.

D. Dopant migration

If we are to believe that two aluminium atoms might be present in adjacent substitutional sites, we must convince ourselves that aluminium can migrate through the lattice at the temperatures that exist during combustion. Unless it was true that dimers could enter the lattice, aluminium atoms must be able to travel through the lattice until they collide with titanium vacancies or other aluminium atoms. It would therefore be instructive to investigate the likelihood of such a migration process taking place, where aluminium is expected to migrate through the lattice as an interstitial Al^{3+} cation. For this reason interstitial sites in both anatase (Fig. 7) and rutile (Fig. 8) were investigated as were the transition states between adjacent sites. These states were originally investigated as both doublets and quadruplets in order to confirm that interstitial aluminium indeed exists as an Al^{3+} cation. Figure 9 shows the relative energies of the interstitial states and the transition states as calculated in $Ti_{16}O_{32}$ supercells.

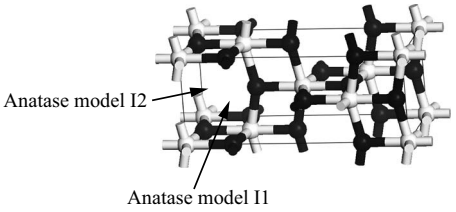

FIG. 7. Interstitial sites in anatase phase TiO_2. The arrows point to the location of the Al atoms. Titanium atoms are white and oxygen atoms are black. The Al atom in anatase model I1 is positioned vertically midway on the front face, in anatase model I2 it is positioned 1/4 of the way through the cell and vertically midway. The figure does not show relaxation due to the presence of Al. Precise geometries are provided as supplementary material (Ref. 64).

1. Anatase

In anatase, two stable interstitial sites were found. Figure 7 shows these two sites. Anatase model I1, where Al is halfway between two oxygen atoms, is more stable than anatase model I2, where Al is at the furthest point from any adjacent atoms. Anatase model I1 is very close to an equivalent site of identical energy between the two next-closest oxygen atoms. There is a negligible energy barrier between these sites (<0.05 eV). For this reason migration around the entire anatase lattice can occur by traversing this one transition state. Unlike in rutile there is no favored orientation of travel. The anatase transition state is 78 kJ/mol higher in energy than anatase model I1. The anatase transition state is 34 kJ/mol higher in energy than anatase model I2.

2. Rutile

As opposed to the work by Steveson *et al.*,[11] we found that in rutile there is effectively only one interstitial site after the lattice is allowed to relax (see Fig. 8). This implies that there are two likely transitions between adjacent sites. Unsurprisingly the barrier to migration in the [110] direction (left and into the page in Fig. 8) is significantly higher than in the [001] direction (up in Fig. 8). Simply put, this is because the latter involves motion through a larger hole. Rutile

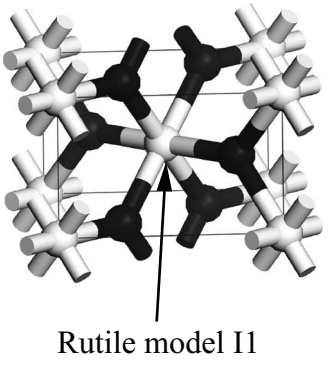

FIG. 8. Interstitial site in rutile phase TiO_2. The arrow points to the location of the Al atom. Titanium atoms are white and oxygen atoms are black. The Al atom in rutile model I1 is located directly in the center of the front face. The figure does not show relaxation due to the presence of Al. Precise geometries are provided as supplementary material (Ref. 64).

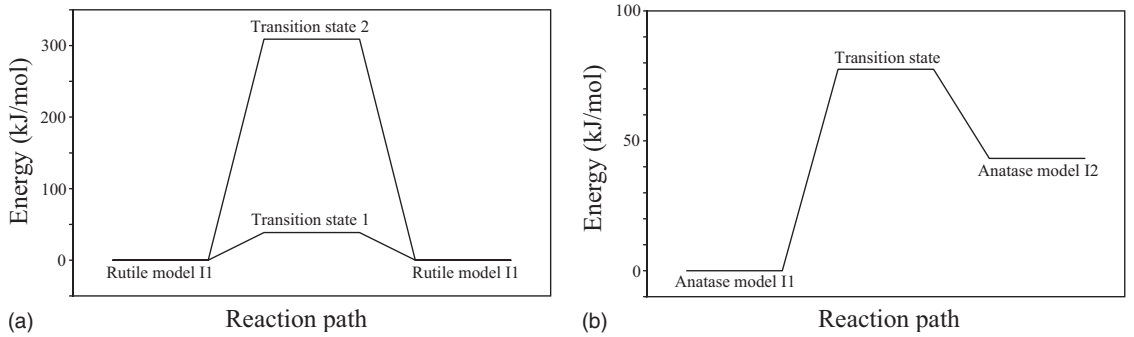

FIG. 9. Transitions states for migration of Al atoms in both the (a) rutile and (b) anatase phases. Precise geometries and energies are provided as supplementary material (Ref. 64).

transition state 1 is 39 kJ/mol higher than rutile model I1. Rutile transition state 2 is 309 kJ/mol higher than rutile model I1. It should be noted that the interstitial site of Al in rutile is effectively that point furthest from any atoms in the lattice. The triplet state of Al is marginally lower in energy than the singlet state (0.002 eV). The same value is found in both of the anatase interstitial models. This is analogous to Al in a vacuum.

V. DISCUSSION

We have demonstrated that DFT simulations give reliable results for the energy, geometry, and bulk properties of TiO_2. While this theory is known to underpredict band gaps we have shown that it gives qualitatively similar answers to the hybrid functionals used by Islam *et al.*[12] Hybrid functionals have not been entirely embraced by the solid-state community because they are more expensive with plane-wave basis sets than with the Gaussian-type orbitals used for molecular calculations. It is instructive to see how calculated properties depend on the assumed defects. The calculations reported here involve far higher Al concentrations than those in industrially produced TiO_2. However, we have shown that the interaction between adjacent defect states in our supercells is low; around 20 kJ/mol. Going to lower concentrations would therefore not be the best use of resources.

It is assumed that Al doping reduces photoactivity not just because it pushes the absorption edge further in to the UV but also because the defects act as recombination centers. The question of why these defect states are such effective recombination centers remains. Doping with nitrogen, carbon, or boron tends to involve substitution with an oxygen atom and has been shown to reduce the band gap and to increase photoactivity. It may be that the aluminium acts to stabilize the oxygen vacancies and that it is the oxygen vacancies and not merely the presence of a defect that increases recombination.

Results suggest that, at industrially relevant temperatures, migration of Al takes place in rutile but not in anatase. The energy of the anatase transition state (78 kJ/mol) corresponds to the thermal energy at around 9300 K. This is essentially insurmountable whereas in rutile, the lower transition state is at 39 kJ/mol corresponding to around 4600 K; still high but possible to overcome at industrial temperatures of 3000 K. Additionally, the relaxed interstitial sites are significantly less stable in anatase, by over 100 kJ/mol. This may be important for phase determination because Al migration is required in order for the more stable defect states with two adjacent Al atoms to form. The states will form faster in rutile than in anatase because the Al will be able to hop from site to site until it collides with a Ti or O vacancy.

VI. CONCLUSIONS

The electronic structure of both anatase and rutile TiO_2 is calculated using the CASTEP DFT software package. After a convergence study with respect to the electronic energy and band gap, a PBE functional is chosen with a basis-set cutoff energy of 380 eV. The effect of aluminium doping on the band gap of the anatase phase has been determined. Calculations of optical properties of the defect states of rutile and anatase have also been carried out. Results are displayed for various defect states of anatase including oxygen vacancies. Calculations of rutile defects have also been made in order to validate the method applied here. Additionally, the transition of interstitial aluminium atoms through the anatase and rutile latices is investigated.

(1) The lowest energy of the conduction band is raised by aluminium doping in both anatase and rutile TiO_2. Although in single substitution states aluminium effectively inserts an electronic state above the top of the valence band leading to a reduction in the band gap and turning the material into a conductor.

(2) Aluminium doping leads to a lowering of the refractive index overall across the visible. This trend is the same for both rutile and anatase phase TiO_2. Single substitution will turn the material into a conductor and the absorption will be nonvanishing at long wavelengths.

(3) Both phases are stabilized by aluminium doping. In order to understand the reasons for it promoting rutile during the combustion synthesis it is necessary to understand more about the nucleation process.

(4) Migration of aluminium atoms in rutile is significantly easier than in anatase. Al migration is unlikely in anatase at industrially relevant temperatures. Migration in rutile has a favored direction of travel, [001], in anatase there is no such preference.

ACKNOWLEDGMENTS

We thank TiOxide Europe Limited (TEL) for the financial support of R.S., the Martin Smith Foundation for the financial support of O.R.I., and the EPSRC for help in the form of research hopping Grant No. EP/E01724X-1. We also express our gratitude to Heidelberg University for providing generous access to the HELICS high-performance computing service.

*mk306@cam.ac.uk; http://como.cheng.cam.ac.uk/mk306

[1] J. Emsley, *Molecules at an Exhibition* (Oxford University Press, New York, 1999).
[2] R. A. Gonzalez, C. D. Musick, and J. N. Tilton, U.S. Patent No. 5508015 (1996).
[3] J. C. Deberry, M. Robinson, M. Pomponi, A. J. Beach, Y. Xiong, and K. Akhtar, U.S. Patent No. 6387347 (2002).
[4] R. H. West, M. S. Celnik, O. R. Inderwildi, M. Kraft, G. J. O. Beran, and W. H. Green, Ind. Eng. Chem. Res. **46**, 6147 (2007).
[5] R. H. West, R. A. Shirley, M. Kraft, C. F. Goldsmith, and W. H. Green, Combust. Flame **156**, 1764 (2009).
[6] R. D. Shannon and J. A. Pask, J. Am. Ceram. Soc. **48**, 391 (1965).
[7] R. Rodríguez-Talavera, S. Vargas, R. Arroyo-Murillo, R. Montiel-Campos, and E. Haro-Poniatowski, J. Mater. Res. **12**, 439 (1997).
[8] M. K. Akhtar, S. E. Pratsinis, and S. V. R. Mastrangelo, J. Mater. Res. **9**, 1241 (1994).
[9] S. Vemury and S. E. Pratsinis, J. Am. Ceram. Soc. **78**, 2984 (1995).
[10] R. Shirley, Y. Liu, T. S. Totton, R. H. West, and M. Kraft, J. Phys. Chem. A **113**, 13790 (2009).
[11] M. Steveson, T. Bredow, and A. R. Gerson, Phys. Chem. Chem. Phys. **4**, 358 (2002).
[12] M. M. Islam, T. Bredow, and A. Gerson, Phys. Rev. B **76**, 045217 (2007).
[13] L. D. Finkelstein, E. I. Zabolotzky, M. A. Korotin, S. N. Shamin, S. M. Butorin, E. Z. Kurmaev, and J. Nordgren, X-Ray Spectrom. **31**, 414 (2002).
[14] W. Göpel, J. A. Anderson, D. Frankel, M. Jaehnig, K. Phillips, J. A. Schäfer, and G. Rocker, Surf. Sci. **139**, 333 (1984).
[15] N. Vast, L. Reining, V. Olevano, P. Schattschneider, and B. Jouffrey, Phys. Rev. Lett. **88**, 037601 (2002).
[16] M. H. Mohamed, H. R. Sadeghi, and V. E. Henrich, Phys. Rev. B **37**, 8417 (1988).
[17] L. A. Grunes, R. D. Leapman, C. N. Wilker, R. Hoffmann, and A. B. Kunz, Phys. Rev. B **25**, 7157 (1982).
[18] F. M. F. de Groot, M. Grioni, J. C. Fuggle, J. Ghijsen, G. A. Sawatzky, and H. Petersen, Phys. Rev. B **40**, 5715 (1989).
[19] G. van der Laan, Phys. Rev. B **41**, 12366 (1990).
[20] L. A. Grunes, Phys. Rev. B **27**, 2111 (1983).
[21] L. D. Finkelstein, E. Z. Kurmaev, M. A. Korotin, A. Moewes, B. Schneider, S. M. Butorin, J-H. Guo, J. Nordgren, D. Hartmann, M. Neumann, and D. L. Ederer, Phys. Rev. B **60**, 2212 (1999).
[22] J. C. Woicik, E. J. Nelson, L. Kronik, M. Jain, J. R. Chelikowsky, D. Heskett, L. E. Berman, and G. S. Herman, Phys. Rev. Lett. **89**, 077401 (2002).
[23] P. Kowalczyk, F. R. McFeely, L. Ley, V. T. Gritsyna, and D. A. Shirley, Solid State Commun. **23**, 161 (1977).
[24] H. Mathieu, J. Pascual, and J. Camassel, Phys. Rev. B **18**, 6920 (1978).
[25] R. H. Tait and R. V. Kasowski, Phys. Rev. B **20**, 5178 (1979).
[26] A. Amtout and R. Leonelli, Phys. Rev. B **51**, 6842 (1995).
[27] U. Diebold, Surf. Sci. Rep. **48**, 53 (2003).
[28] S. B. Sinnott, R. F. Wood, and S. J. Pennycook, Phys. Rev. B **61**, 15645 (2000).
[29] K. M. Glassford and J. R. Chelikowsky, Phys. Rev. B **46**, 1284 (1992).
[30] K. M. Glassford, N. Troulier, J. L. Martins, and J. R. Chelikowsky, Solid State Commun. **76**, 635 (1990).
[31] D. C. Allan and M. P. Teter, J. Am. Ceram. Soc. **73**, 3247 (1990).
[32] C. Lee, P. Ghosez, and X. Gonze, Phys. Rev. B **50**, 13379 (1994).
[33] E. Cho, S. Han, H.-S. Ahn, K.-R. Lee, S. K. Kim, and C. S. Hwang, Phys. Rev. B **73**, 193202 (2006).
[34] B. Silvi, N. Fourati, R. Nada, and C. R. A. Catlow, J. Phys. Chem. Solids **52**, 1005 (1991).
[35] N. I. Medvedeva, V. P. Zhukov, M. Ya. Khodos, and V. A. Gubanov, Phys. Status Solidi B **160**, 517 (1990).
[36] M. A. Khan, A. Kotani, and J. C. Parlebas, J. Phys.: Condens. Matter **3**, 1763 (1991).
[37] B. Poumellec, P. J. Durham, and G. Y. Guo, J. Phys.: Condens. Matter **3**, 8195 (1991).
[38] P. K. Schelling, N. Yu, and J. W. Halley, Phys. Rev. B **58**, 1279 (1998).
[39] S. Munnix and M. Schmeits, Phys. Rev. B **30**, 2202 (1984).
[40] N. Daude, C. Gout, and C. Jouanin, Phys. Rev. B **15**, 3229 (1977).
[41] S. Clark, M. Segall, C. Pickard, P. Hasnip, M. Probert, K. Refson, and M. Payne, Z. Kristallogr. **220**, 567 (2005).
[42] L. Liborio and N. Harrison, Phys. Rev. B **77**, 104104 (2008).
[43] O. Inderwildi and M. Kraft, ChemPhysChem. **8**, 444 (2007).
[44] M. Long, W. Cai, Z. Wang, and G. Liu, Chem. Phys. Lett. **420**, 71 (2006).
[45] S. Matsushima, K. Takehara, H. Yamane, K. Yamada, H. Nakamura, M. Arai, and K. Kobayashi, J. Phys. Chem. Solids **68**, 206 (2007).
[46] J. P. Perdew, K. Burke, and M. Ernzerhof, Phys. Rev. Lett. **77**, 3865 (1996).
[47] D. Vanderbilt, Phys. Rev. B **41**, 7892 (1990).
[48] H. J. Monkhorst and J. D. Pack, Phys. Rev. B **13**, 5188 (1976).
[49] *CRC Handbook of Chemistry and Physics*, 77th ed., edited by David R. Lide (CRC, Boca Raton, 1997).
[50] A. Fahmi, C. Minot, B. Silvi, and M. Causá, Phys. Rev. B **47**, 11717 (1993).
[51] S. D. Mo and W. Y. Ching, Phys. Rev. B **51**, 13023 (1995).
[52] R. W. G. Wyckoff, *Crystal Structures* (Interscience, New York, 1963), Vol. 1.
[53] *NIST Chemistry WebBook*, NIST Standard Reference Database

No. 69, edited by P. J. Linstrom and W. G. Mallard (National Institute of Standards and Technology, Gaithersburg, MD, 2005), p. 20899; http://webbook.nist.gov

[54] H. Tang, H. Berger, P. E. Schmid, F. Lévy, and G. Burri, Solid State Commun. **87**, 847 (1993).

[55] N. Govind, M. Petersen, G. Fitzgerald, D. King-Smith, and J. Andzelm, Proceedings of the Symposium on Software Development for Process and Materials Design [Comput. Mater. Sci. **28**, 250 (2003)].

[56] J. F. Stebbins, I. Farnan, and U. Klabunde, J. Am. Ceram. Soc. **72**, 2198 (1989).

[57] A. Seidl, A. Görling, P. Vogl, J. A. Majewski, and M. Levy, Phys. Rev. B **53**, 3764 (1996).

[58] E. Finazzi, C. Di Valentin, and G. Pacchioni, J. Phys. Chem. C **113**, 220 (2009).

[59] V. I. Anisimov, F. Aryasetiawan, and A. I. Lichtenstein, J. Phys.: Condens. Matter **9**, 767 (1997).

[60] M. Cococcioni and S. de Gironcoli, Phys Rev. B **71**, 035105 (2005).

[61] V. Perebeinos and T. Vogt, Phys. Rev. B **69**, 115102 (2004).

[62] C. R. Bradley and A. P. Cracknell, *The Mathematical Theory of Symmetry in Solids* (Oxford, New York, 1972).

[63] C. Qiang and C. Hong-Hong, Chin. Phys. **13**, 2121 (2004).

[64] See supplementary material at http://link.aps.org/supplemental/10.1103/PhysRevB.81.075111 for precise geometries and energies for all the models presented here.

[65] K. Iijima, M. Goto, S. Enomoto, H. Kunugita, K. Ema, M. Tsukamoto, N. Ichikawa, and H. Sakama, Proceedings of the 16th International Conference on Dynamical Processes in Excited States of Solids [J. Lumin. **128**, 911 (2008)].